COMPREHENSIVE REPORT ON LOW TEMPERATURE SOLDER ALLOYS FOR PORTABLE ELECTRONICS

Morgana Ribas, Ph.D.
Anil Kumar
Ranjit Pandher, Ph.D.
Rahul Raut
Sutapa Mukherjee
Siuli Sarkar, Ph.D.
Bawa Singh, Ph.D.
Alpha
South Plainfield, NJ, USA 07080
ssarkar@alent.com

ABSTRACT
We present here the findings of Alpha's Alloy Development Program on the next generation of low temperature alloys that can be used in reflow soldering temperatures from 170 to 200°C. Approaches in alloy development, test methodologies and results are discussed. The alloy properties targeted for improvements include: Alloy strength, alloy ductility, microstructure stability, improvements in thermal cycling, high temperature creep and drop shock. We show how the use of micro-additives in eutectic Sn-Bi alloys improves these properties. Further, comprehensive reliability studies were undertaken for new low temperature alloys. Thermal Cycling was undertaken from -40°C to +125°C with a 10 minute dwell time.

Compared to standard Sn-Bi systems, improvements in thermal fatigue resistance are discussed. The basic properties of the new alloys shown here were fully characterized and their use in SMT applications evaluated, especially in drop shock and temperature cycling tests.

In summary, we present here a new generation of low temperature Pb-free alloys, which are capable of delivering high reliability performance at low soldering temperatures. Various alloy compositions were evaluated and alloy B showed superior performance versus the benchmark and other low temperature alloys. Overall, the new low temperature alloys show significant improvements in metallurgical properties, soldering properties for SMT assembly, and thermal and mechanical reliability.

Key words: Pb-free solders, low temperature alloys, drop shock, thermal cycling.

INTRODUCTION
Progressive miniaturization and increasing complexity of portable electronic devices has imposed a shift in reliability requirements of solders. Improved thermal fatigue and mechanical shock properties grow into must have requirements as thermal management and drop shock resistance of such devices becomes more challenging. As a result, suppliers of solder alloys and interconnecting materials face growing demands on how to maintain or improve existing reliability requirements. Additionally, multi-step assembly process and a surge in use of temperature sensitive components bring in additional challenges.

Alpha Low Temperature Alloys initiative dates back to 2010, when we selected Sn-Bi alloys as the most promising candidates for low temperature soldering. The eutectic Sn-Bi alloy was one of the initial alloys evaluated to replace Sn-Pb as it enables reflow soldering temperatures of 170-190°C, has low cost and can be used in the assembly of temperature-sensitive applications. Use of such low reflow temperatures results in lower thermal stresses and defects such as warping during assembly. However, eutectic Sn-Bi is also known to have poor thermal cycling performance and lower ductility [1-5]. Such poor elasticity and plasticity is likely to result in lower ability of the solder joint to withstand impact and poor drop shock properties.

The eutectic Sn42-Bi58 alloy has a melting point of 138°C. Reducing the Bi content to 40 wt% increases the liquidus temperature to about 170°C. Such a wide melting range is sometimes seen with skepticism in solders for SMT applications because it can result in various assembly defects. Besides the melting point, the most notable is the variation in its mechanical properties. Sn60-Bi40 has a slightly lower ultimate tensile strength, but its elongation at break significantly increases more than 100% [1, 6-7]. Very little work has been done on the board level drop shock performance of such alloys. A previous study [7] shows that the drop shock characteristic life (63% failures) of these alloys increases as the Bi content decreases from 58 to 40 wt%. However, irrespective of the Bi content of the alloy, a large number of early failures (below 10 drops) is observed. Either due to their brittleness or the increased number of defects in the off-eutectic alloys, such results indicate that a series of drawbacks of Sn-Bi alloys need to be addressed in order to make them suitable for electronic soldering applications.

Originally published in the Proceedings of the SMTA International, Rosemont, IL, September 27 - October 1, 2015

Here we present a comprehensive report on our Low Temperature Alloys initiative. By means of various alloying additions, we show how to improve drop shock and thermal cycling performance of Sn-Bi alloys. In addition, we show how basic properties, mechanical properties and solder paste performance of these new alloys support these findings.

EXPERIMENTAL METHODOLOGY

Thermal Analysis

The liquidus and solidus temperature of the alloys was measured using a differential scanning calorimeter (DSC), as per ASTM E794 standard. The coefficient of thermal expansion (CTE) was measured using a thermal mechanical analyzer from TA Instruments (model TMA2940), according to the RT-500C standard.

The thermal diffusivity of the alloys was measured using a Netzsch LFA447 Nanoflash instrument. In this, a Xenon flash emits a light pulse that heats the front side of the sample and results on a temperature signal versus time on the rear surface, which is measured using an infrared detector. This temperature distribution depends on the thermal diffusivity (α) of the material, which was then used to calculate the thermal conductivity (K) as, $K=\rho\ \alpha\ c_p$, where ρ is the density and c_p the specific heat.

Molten Solder Evaluation

The wetting balance test of the alloys was carried out on Cu substrates, in accordance to the JIS Z 3198-4 standard. The tests were performed using a Rhesca solder checker to report the zero wetting time (t_0) and maximum force (F_{max}). The 30 x 10 x 0.30 mm Cu coupons were cleaned and completely immersed in RF 800 flux and allowed to dry for 10s. The coupons were then immersed to a depth of 4-5mm in the molten alloy at a speed of 20mm/s and held for 10s. Tests were performed at 190°C.

A typical wetting balance curve shows the variation of the wetting force of the solder on a test vehicle surface with respect to time (Figure 1). Basically, six distinct events can be identified during the wetting test: (A) The initial stage just before immersion in the solder, (B) As the test vehicle is immersed in the solder, there is an opposite (negative) force applied by the solder on the surface, (C) The wetting force increases and returns to zero upon wetting (t_0), (D) The wetting force increases and reaches its maximum value (F_{max}) as the test vehicle withdraws from the molten solder, (E) The wetting force increases again at the minimum contact of the test vehicle with the solder, (F) The wetting force decreases as the test vehicle is completely removed from the solder. So, a lower zero wetting time and higher wetting force are desirable properties for an alloy.

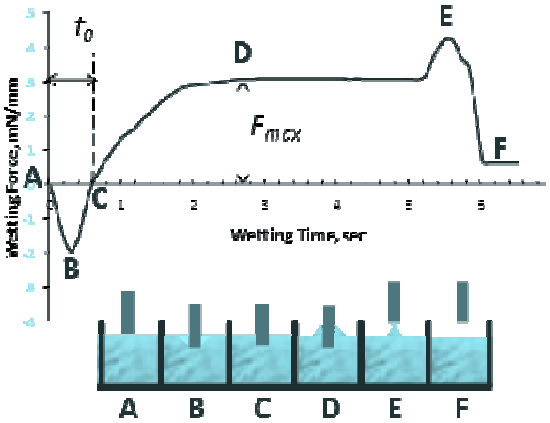

Figure 1. Schematic wetting balance curve

The copper dissolution is assessed by measuring the time taken for a wire to break under load when immersed in solder. For this test, a 0.05 mm diameter copper wire was fluxed with RF800 flux and dipped in molten solder, which was kept at 190°C. The copper dissolves in the solder and after a given time it has insufficient strength to support the weight attached to it. This procedure was repeated multiple times for each alloy and the rate of copper dissolution was calculated for the time it took the copper to dissolve.

Mechanical Properties Testing

Tensile tests were conducted using an Instron universal testing machine - Model 5566 (Figure 2). Rounded specimens were prepared as per ASTM E8 tensile test standard (16 mm gauge length and 4mm gauge diameter) and the tests were performed at room temperature and 10^{-3}mm/s strain rate for at least five specimens of each alloy. The average values of ultimate strength, yield strength, elastic modulus and elongation were reported.

(a)

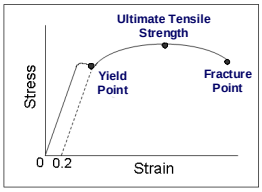

(b)

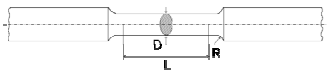

Diameter (D)	Gage Length (L)	Shoulder radius (R)
4mm	16mm	3mm

(c)

Figure 2. (a) Instron universal testing machine with environmental chamber, (b) Stress-strain curve schematics and (c) Test specimen geometry used for tensile testing

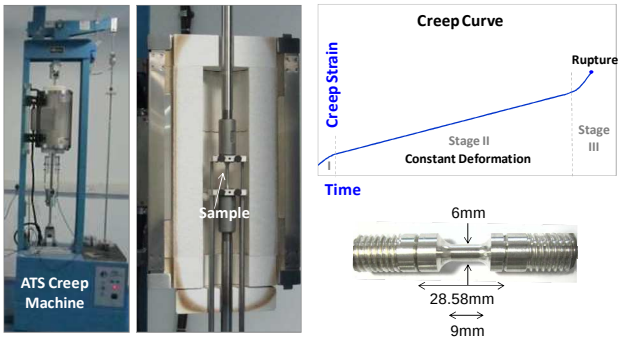

Figure 3. Left: Creep machine. Right: Schematic creep curve (top) and creep test specimen (bottom)

For the Creep test, cylindrical specimens of 9 mm gauge length and 6 mm diameter (Figure 3) were machined and baked at 80°C for 48 hrs prior to testing. The test was performed using an ATS creep machine 2320, using 150N load, at 80°C. Creep strength and creep elongation average values of at least three replicates of each alloy are reported.

An ultrasonic pulse-echo technique is used to evaluate the elastic properties of the alloys without the variability often observed when performing tensile tests. An Olympus 38DL PLUS ultrasonic thickness gage, and longitudinal and shear wave transducers is used to measure the sound velocities through the alloys, which are then used to compute their Young's Modulus, Shear Modulus and Poisson's ratio.

Mechanical strength of the solder joints was measured using shear test of chip resistors conducted on a DAGE 4000 system, as per the JIS Z3198-7:2003 standard. Components were assembled using a paste made with Alpha CVP520 flux and type 4 solder powder of the solder alloys. The shear force was measured on 20-25 #1206 chip resistors at 700 µm/s shear speed and 20 µm shear height.

Solder Paste Evaluation

Test vehicles used in this study were reflowed in a seven zone heater reflow machine (Ominiflo7); soak at 100-120°C for 90 sec, 180°C peak and 60 sec time above liquidus. Random solder balls (RSB) were evaluated using ceramic coupons, JIS spread and JIS hot slump test used copper coupons, whereas wetting, mid chip solder ball (MCSB), coalescence and joint cosmetics were evaluated using CERF boards (Figure 4). Chip resistors of various sizes were assembled on this test vehicle and used to evaluate shear strength, solder joint microstructure features and intermetallic compound thickness.

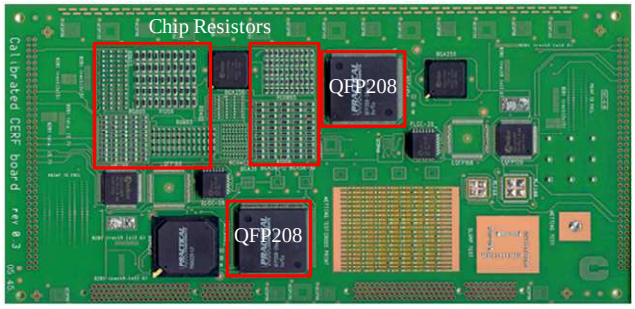

Figure 4. Calibrated CERF board used to evaluate solder paste performance

Drop Shock

The effect of drop and shock on handheld devices is best evaluated by assembly of actual devices that are then "dropped" following a defined testing protocol. However, these are quite cumbersome and expensive tests to be conducted, and as such, not viable to be used in solder alloys development. The solution is to use proxy tests at board level. Among those, the JEDEC drop shock test is perhaps the most used test, as it provides guidelines on test vehicle and testing protocol that makes it easier to compare test results across various alloys independently on the equipment utilized.

JESD22-B111 standard is used to evaluate corresponding board level drop shock resistance of handheld devices. A Lansmont M23 shock machine, shown in Figure 5(a), is used for performing the drop tests of our customized test vehicle, Figure 5(b). Test Vehicle follows the JEDEC recommendation and uses CTBGA84 components with 84 I/Os with 0.5 mm pitch and 0.3 mm diameter spheres. Pad finish on the component side is NiAu and on the board side is Cu-OSP. By adjusting the drop height and the strike surface it is possible to achieve JEDEC's recommended service condition B (1500Gs, 0.5 msec duration and half-sine pulse), which is monitored as shown in Figure 5(c).

The test vehicle used for drop shock and thermal cycling tests is a Cu-OSP finished board with non-solder mask defined 0.225 mm pads, as shown in Figure 5(b). Each board can accommodate up to 15 BGA84, which are individually monitored for electrical discontinuities. For the results shown here all BGA84 components had Sn-Ag3-Cu0.5 spheres.

The electrical continuity of each component is monitored during each drop using an Analysis Tech STD event detector. Each of the BGA84 assembled in the drop shock test vehicle was tested till failure (electrical resistance discontinuity greater than 1000 Ω lasting more than 1 µsec). The BGA failures were recorded once a first discontinuity is followed by three others within five subsequent drops. Weibull probability distribution was used to analyze the number of drops to failure data. .

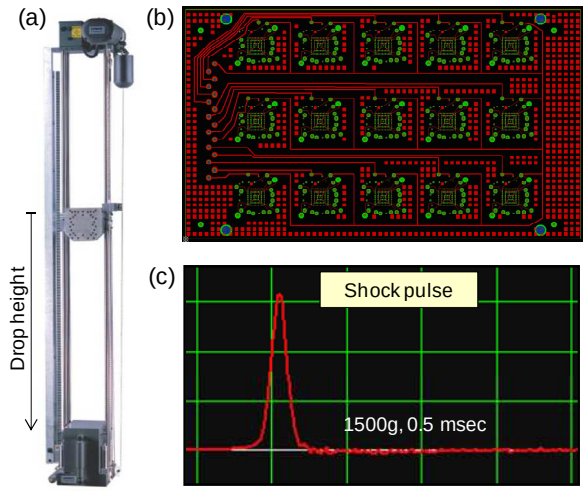

Figure 5. (a) Lansmont drop shock testing machine, (b) Alpha drop shock test vehicle and (c) half-sine shock pulse curve corresponding to JEDEC service condition B

Thermal Cycling

Thermal cycling test was performed as per the IPC9701 standard, from -40°C to +125°C, with 10 min dwell time. A thermal shock chamber from (Espec model TSA-101S) capable of fast heating and cooling rates was used for the testing. The test vehicle has fifteen CTBGA84 that were electrically monitored for discontinuities/increase in contact resistance using an Agilent data logger (model 34980A).

RESULTS AND DISCUSSION

Thermal Properties

Standard Sn-Bi alloy systems have a melting temperature of 138°C. This enables soldering temperatures to be limited to 170-200°C, avoiding any thermal damage to the soldered electronic components. A lower melting point is also desirable as it results in cost savings through lower power consumption. Additionally, a narrow solidus and liquidus temperature range was preferred for the candidate alloys as it favors the soldering process and, in the case of Sn-Bi system, results in cosmetically preferable solder joints. Table 1 shows the three selected alloys with melting temperatures very close to Sn42Bi58 alloy, about 138°C.

Table 1. Melting temperature, coefficient of thermal expansion (CTE) and thermal conductivity of the alloys

Alloy	Melting Temp (^oC)	CTE (ppm/^oC)	Thermal Conductivity (W/mK)
Sn42-Bi58	138.1	16.7	21.6
Sn-Bi57.6-Ag0.4	137.4	17.1	24.5
A	138.6	16.7	25.6
B	138.5	17.1	25.5
C	137.4	17.6	24.6

The CTE value is a critical attribute as it determines solder joint's integrity under thermal fatigue. It is well-known that the formation of intermetallic compounds characterizes the nature of the metallurgical bond, but due to their brittle nature they can also lead to joint failure when there is an excessive mismatch between the CTE of solder and board/components. Since crystallographic structure of IMCs is different than that of the solder, they raise stress locally, and provide potential sites for crack initiation under thermal fatigue. As shown in Table 1, the CTE of alloys A, B and C is between 16.7 and 17.6 ppm/°C, which is very similar to other Sn-Bi alloys such as Sn42Bi58 and Sn42Bi57.6Ag0.4.

From a functional standpoint, alloys with higher thermal conductivity are always preferred, especially when used to solder high-power electronics components. However increasing the thermal conductivity depends not only on the conductivity of the added elements but also on how they affect the alloy microstructure and the final heat conduction path. An addition of 0.4 wt% Ag to Sn42Bi58 has a significant effect on the thermal conductivity, which increases by about 13% (Table 1). The thermal conductivity of alloy A is identical to Sn42Bi57.6Ag0.4, whereas for alloys B and C it increases by about 18%.

Molten Solder Properties

The wetting curves of the alloys evaluated were similar for the given test conditions (e.g., test vehicle surface finish, type of flux and pot temperature). Wetting time (t_0) of alloys A, B and C is slightly lower than Sn42Bi58 and SnBi57.6Ag0.4. The maximum wetting force of these alloys is basically identical, reinforcing the impression that the wetting behavior of these alloys is almost similar under the given test conditions.

Low copper dissolution is preferred to avoid deterioration of the solder joint. The rate of copper dissolution of the alloys evaluated is shown in Table 2. Sn42Bi57.6Ag0.4 has the highest rate of copper dissolution (12.5 μm/min), whereas alloys A and B have very low rate of copper dissolution (0.24 μm/min), which is about 40.8 times lower than Sn42Bi58 and 52 times lower than Sn42Bi57.6Ag0.4 alloys. Alloy C, which also contains Ag, also shows much lower copper dissolution (2.3 μm/min) than Sn42 Bi57.6Ag0.4, which was achieved through a secondary alloy addition.

Table 2. Zero wetting time (t_0), maximum wetting force (F_{max}) and copper dissolution rate

Alloys	t_0 (sec)	F_{max} (mN)	Cu Dissol. (μm/min)
Sn42Bi58	1.62	3.63	9.8
Sn42Bi57.6Ag0.4	1.42	3.82	12.5
Alloy A	1.32	3.77	0.24
Alloy B	1.07	3.72	0.24
Alloy C	1.26	3.76	2.3

Mechanical Properties

Typical stress-strain curves of the alloys evaluated are shown in Figure 6. For each alloy, at least three replicas

were tested and the average tensile properties were recorded and shown in Table 3. The addition of Ag to the Sn42Bi58 alloy resulted in a 6% higher ultimate tensile strength. Other elemental additions resulted in further improvement of the ultimate tensile strength – 15% for alloy A, 10% for alloy B and 9% for alloy C. Overall, minor alloying additions of Ag and other elements to Sn42Bi58 improve the tensile properties of the alloys. Indeed, the other alloying additions used in alloys A, B and C resulted in higher alloy strengthening than Ag addition alone.

Typically, an alloy with higher modulus will be stiffer, i.e., less flexible under tension and, will have lower elongation. An ideal alloy composition should have sufficient modulus without compromising its ductility and elongation. Although the elastic modulus does not vary much with the various alloying additions, alloys A and B have significant higher elongation.

Another useful property that can be correlated to the toughness and ductility of the alloy is breaking energy in the Charpy Impact Test. In this test, a pendulum with known weight hits the sample (as shown in the schematics of Figure 7). Energy of the pendulum lost to break the sample is measured. Charpy Impact Test results are shown in Fig 7. Alloys A and B have about 5-7% higher Charpy impact energy as compared to Sn42Bi58 and Sn42Bi57.6Ag0.4 alloys. Alloy C has the impact energy equivalent to 0.4 wt% Ag addition.

Table 3. Ultimate tensile strength (UTS), yield strength (YS), elongation and Young's modulus (*E*) of Sn-Bi58 Plus alloys

Alloys	UTS (MPa)	YS (MPa)	Elongation (%)	$E^{\#}$ (GPa)
Sn42Bi58	63.6	53.0	48.2	39.0
SnBi57.6Ag0.4	67.4	58.3	52.6	39.3
Alloy A	73.0	59.4	69.8	38.8
Alloy B	70.2	60.1	66.1	39.1
Alloy C	69.4	58.2	51.8	39.0

$^{\#}$Measured by ultrasonic pulse-echo technique.

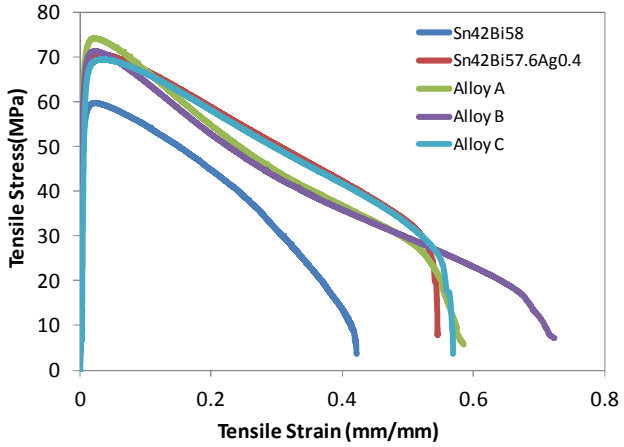

Figure 6. Typical stress-strain curves of the alloys

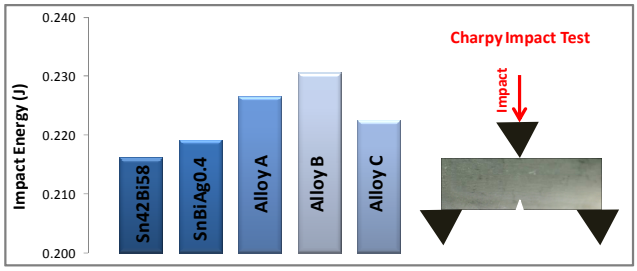

Figure 7. Impact energy from Charpy test (Left) and schematics of the test (Right)

Typical creep curves of the alloys evaluated are shown in Figure 8. Three stages are usually observed in a creep curve: I is dominated by strain hardening, in II the strain hardening is balanced by the annealing resulting in an almost constant deformation, and in III necking and the ultimate rupture occur. In the curves shown below the primary stage is very short and the minimum creep rate happens at low strain levels. Secondary stage is usually the longest, as shown below, but the tertiary stage also has a predominant contribution during the creep process.

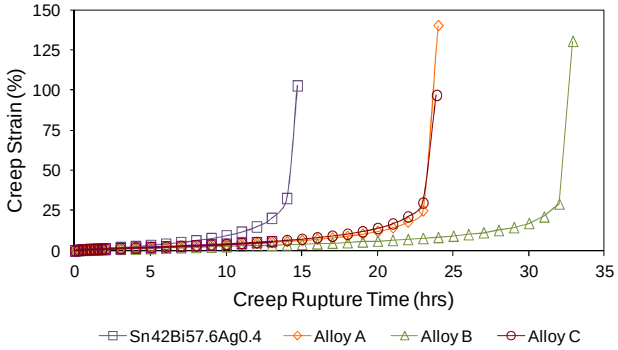

Figure 8. Typical creep curves of the alloys evaluated

Average values of creep rupture time and creep strain are shown in Table 4. The creep rupture time indicates the creep strength, whereas the creep strain indicates the creep elongation. Elongation and resistance are often in opposite sides of a balance, i.e., the increase in strength quite often results in loss of elongation. However, it is important to ensure that the new alloys do not trade much of their elongation for strength. Sn42Bi57.6Ag0.4 and alloys A, B and C have comparable elongation. However, the minor addition present in alloys A, B and C result in remarkable improvement over Sn42Bi57.6Ag0.4 creep strength.

Table 4. Creep rupture time and creep strain at 85°C and 150 N load

Alloys	Creep Rupture Time (hrs)	Creep Strain (%)
Sn42Bi57.6Ag0.4	14.0	99.3
Alloy A	20.5	112.9
Alloy B	25.4	107.4
Alloy C	18.8	110.6

Although the mechanical properties alone are not sufficient to predict drop shock behavior of an alloy, they serve as a good indication of its performance. In this case, tensile properties and Charpy impact energy results were useful to indicate the superior drop shock performance of alloys A and B. In addition to that, high temperature creep properties provide useful insight into thermal fatigue performance of the alloys, as it will be seen in the following sections.

Solder Paste Evaluation

Sn42Bi58 and Sn42Bi57.6Ag0.4 solder powders are available commercially, whereas experimental batches of IPC type 4 powders were initially manufactured with alloys A, B and C for this study. ALPHA CVP520 paste flux was used to prepare the solder pastes analyzed here. Paste attributes and printing performance were evaluated, including: Spread/wetting, coalescence, hot and cold slump, voids, flux residue and joint cosmetics.

For the IPC RSB test, all pastes meet the IPC acceptance criteria for immediate reflow and 4hrs conditioning at 25°C/50% RH. The IPC slump test evaluates the ability of a solder paste to maintain its shape under two controlled environments. The results of the IPC slump test show that all pastes meet the IPC acceptance criteria for hot and cold slump based on standard ANSI/J-STD-005. The JIS slump test results show that the alloys have equivalent JIS hot and cold slump characteristics.

The cross print test measures the number of shorts as a function of the separation of printed paste traces, so it can also be used to evaluate the paste spread as well as coalescence at the same time. Figure 9 shows the cross print data for the alloys. Overall, Sn42Bi57.6Ag0.4 has the worse spread in the cross print test, whereas Alloy C has the best, with the other pastes falling somewhere in between. Void analysis show that all solder pastes can be classified as CLASS-3 (void less than 9% of area) as per IPC-7095A guidelines. Visual inspection (joint cosmetics) of solder and residue for all solder pastes shows: (i) Flux residue: Light amber color, soft and tacky, (ii) Solder cosmetics: Shiny, (iii) Not observed: De-weting on large, flux burn, cracks in residue and bubbles in flux residue, (iv) Residue amount: Medium and (v) Flux spread: More.

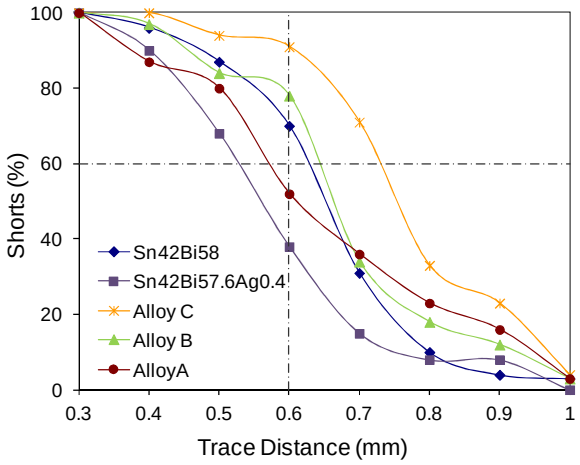

Figure 9. Cross print evaluation of the alloys

Drop Shock Performance

When designing an alloy for improved drop shock performance it is very important to look in to the physical metallurgy of this alloy. Bi forms a solid solution with Sn, resulting in a eutectic alloy with 42 wt% Sn and 58 wt% Bi. As shown in Figure 10, the resulting drop shock characteristic life (63% failures) is very low, about 118 drops). As Ag has limited solubility in the eutectic phase, addition of Ag will form precipitates when added to it. Presence of such precipitates dispersed in the Sn-Bi matrix prevents plastic deformation resulting in its strengthening. Indeed, drop shock characteristic life of Sn42Bi57.6BiAg0.4 is 25% higher than that of Sn42Bi58.

In addition to solid solution and precipitate hardening, diffusion modifiers are another important way to modify the properties of an alloy when considering drop shock performance. The growth of interfacial intermetallics and interfacial voids can be controlled through addition of diffusion modifiers to the solder. Similarly, the mechanical properties of the bulk solder alloy can be controlled through the formation of intermetallics and microstructure refinement. The choice of which alloying element(s) to add depends on its relation with the alloy system and the resulting thermodynamics and kinetics properties. The effect of such additions in the alloy can be verified from tests as simple as shear strength tests to the more complex drop shock tests.

Alloys A and B were designed having these strengthening mechanisms in mind in order to obtain stronger solder joints that would reflect in better drop shock performance. Drop shock characteristic life of alloy A is 62.6% higher than Sn42Bi58 and 30% higher than that of Sn42Bi57.6Ag0.4. Alloy B's characteristic life is 160% higher Sn42Bi58 and 108% higher than that of Sn42Bi57.6Ag0.4. The next question would be if such remarkable strengthening of the solder joint of the eutectic Sn-Bi alloy would affect thermal cycling performance as well. The answer to this is shown in the next section.

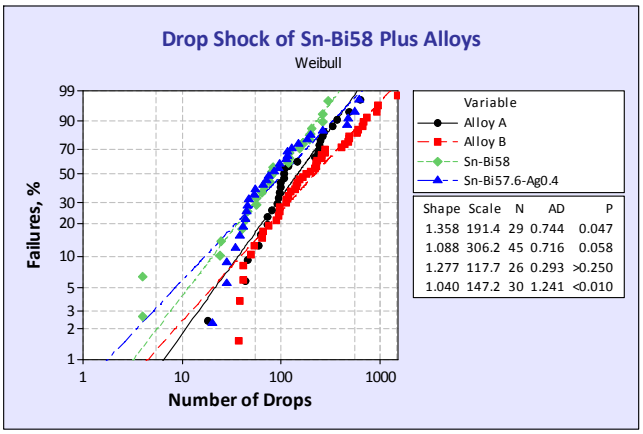

Figure 10. Drop shock performance of the alloys

Thermal Cycling Performance

There are various ways to verify thermal cycling performance of an alloy. If the test is actively monitored, increase in the electrical resistance can be monitored and the % failures given. In addition to that or if the electrical resistance is not monitored, additional solder joints can be cross-sectioned at determined intervals. Besides that, the solder joints post thermal cycling can be tested for shear strength pull strength, vibration resistance etc. Next we look at the thermal cycling performance of Sn42Bi57.6Ag0.4 and alloy B in a few different ways.

Table 5 shows the % failures after certain number of temperature cycles. After 200 thermal cycles. Sn42Bi57.6Ag0.4 presented most of its failures in this interval (17.7%), whereas alloy B showed no failures. The failures in Sn42Bi57.6Ag0.4 progressed to 23.5% in the interval between zero and 800 thermal cycles, achieving its maximum before the test was interrupted. In the case of alloy B, a single component (out of 36) failed in the interval between zero and 1000 thermal cycles. This failure occurred around 500 cycles, but the possibility of this being an outlier cannot be discarded.

The behavior of these alloys under thermal cycling can be confirmed through cross-sectioning and microscopic analysis. One of such examples is shown in Figure 11, in which BGA samples after 200, 500, 800 and 1000 cycles were examined. For Sn42Bi57.6Ag0.4, small cracks were visible in the BGA samples tested from zero to 200 thermal cycles. Progressively larger cracks were observed in the joints tested after longer number of cycles. These images corroborate previously shown results of % failures detected through increase in the BGA electrical resistance. For alloy B, the first identifiable crack was observed in the joints sampled between 500 and 800 thermal cycles. However, this crack is so small that cannot be seen without a high magnification enlargement of the area.

Table 5. Failures (%) detected by electrical resistance measurements in thermal cycling test

Alloys	BGA Failures (%)			
	200 Cycles	500 Cycles	800 Cycles	1000 Cycles
Sn42Bi57.6Ag0.4	17.7	20.6	23.5	23.5
Alloy B	0	2.8	2.8	2.8

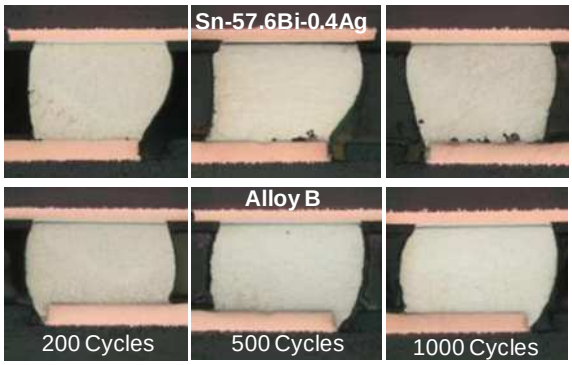

Figure 11. Crack initiation in BGA using Sn42Bi57.6Ag0.4 and alloy B

The effect of thermal cycling on BGA components is generally more pronounced than in chip resistors. However, further information can be gathered on the alloy thermal cycling performance with the evaluation of chip resistors, because unlike in the BGAs evaluated here that form SAC305/Sn-Bi mixed solder joints, the solder joints in the chip resistors are made entirely of the low temperature alloys. Therefore that eliminates any possibility of results being skewed by local change in composition of the solder due to mixing of SAC and Sn-Bi alloys.

Figure 12 shows the effect of thermal cycling on the shear strength of #1206 chip resistors assembled with Sn42Bi57.6Ag0.4 and alloy B. Up to 200 thermal cycles, both alloys have similar behavior and shear strength. Around 500 cycles, Sn42Bi57.6Ag0.4 decrease in shear strength accelerates, becoming clearly visible at 800 thermal cycles. Figure 13 shows cross-sections of the chip resistor solder joints after 200, 500, 800 and 1000 cycles. Both alloys form similar solder fillets indicating both have comparable joint formations. Some voids are visible in both alloys, but cracks were identified much later than in the BGAs. For Sn42Bi57.6Ag0.4 cracks were visible between 800 and 1000 thermal cycles, whereas no cracks were observed for alloy B till 1000 cycles.

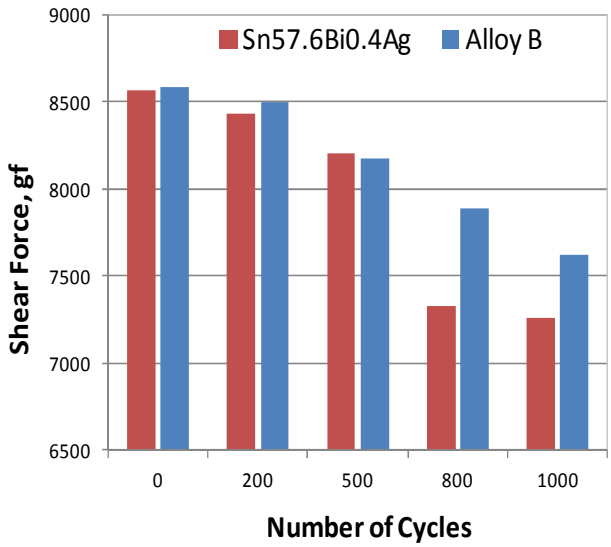

Figure 12. Shear strength of Sn42Bi57.6Ag0.4 and alloy B measured on chip resistors 1206

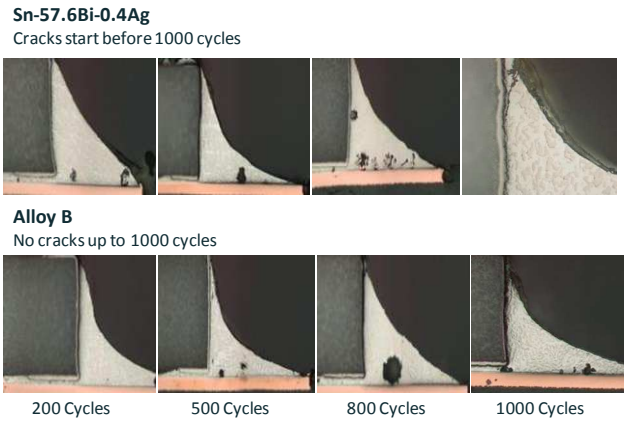

Figure 13. Joint appearance of Sn42Bi57.6Ag0.4 and alloy B on 0603 chip resistors

CONCLUSIONS

To summarize we presented here a comprehensive data generated at every stage of the low temperature alloy development process. Multiple test methods have used to evaluate and understand the solder alloys. Basic mechanical properties and creep behavior of the bulk solder has been used to predict mechanical and thermal fatigue life of the final solder joints. Real life tests have been used to confirm the predictions. New, short listed alloy shows significant improvements in drop shock as well as thermal cycling performance as compared to Sn42Bi58 and Sn42Bi57.6Ag0.4 eutectic alloys. New alloy also shows dramatically lower Cu dissolution rate.

REFERENCES

1. Glazer, J., "Metallurgy of low temperature Pb-free solders for electronic assembly". *Int. Mater. Rev.*, Vol. 40, No. 2 (1995), pp. 65-93.
2. Mei, Z. *et al.*, "Low-Temperature Solders". *Hewlett-Packard Journal*, Article 10, August (1996), pp. 1-10.
3. Hua, F. *et al.*, "Eutectic Sn-Bi as an Alternative Pb-Free Solder". *Proc 48th Electronic Components and Technology Conf.*, Seattle, WA, May. 1998, pp. 277-283.
4. McCormack, M. *et al.*, "Significantly Improved Mechanical Properties of Bi-Sn Solder Alloys by Ag-Doping", *J. Electron. Mater.*, Vol. 26 (1997), pp. 954-958.
5. Miric, A. Z. and Grusd A., "Lead-Free Alloys", *Soldering & Surface Mount Technology*, 10/1 (1998), pp. 19-25.
6. Takao, H. *et al.*, "Mechanical Properties and Solder Joint Reliability of Low-Melting Sn-Bi-Cu Lead Free Solder Alloy". *R&D Review of Toyota CRDL*, Vol. 39, No. 2 (2004), pp. 49-56.
7. Ribas, M. et al., "Development of Low-Temperature Drop Shock Resistant Solder Alloys for Handheld Devices", Proc. IEEE 15th Electronics Packaging Technology Conference, Singapore, Dec. 2013.

Originally published in the Proceedings of the SMTA International, Rosemont, IL, September 27 - October 1, 2015